In-Situ Diagnostic Tools for Hydrogen Transfer Leak Characterization in PEM Fuel Cell Stacks Part III: Manufacturing Applications

Amir M. Niroumand[1,*], Hooman Homayouni[2], Gert Goransson[3], Mark Olfert[2], and Michael Eikerling[1]

1- Department of Chemistry, Simon Fraser University, 8888 University Drive, Burnaby, BC, V5A 1S6, Canada
2- Greenlight Innovation, 104A–3430 Brighton Ave, Burnaby, BC, V5A 3H4, Canada
3- PowerCell Sweden AB, Ruskvädersgatan 12, SE-418 34 Gothenburg, Sweden

Abstract

This work describes a novel diagnostic technique for detection and isolation of manufacturing defects in polymer electrolyte fuel cell stacks. Two of the main causes of early stack failure are membrane pinholes and electric shorts. Membrane pinholes result in the local hydrogen crossover from anode to cathode, which reduces fuel utilization. With the growth of the pinhole, the crossed over hydrogen exits the cathode as hydrogen emission. When this emission passes the safe lower explosion limit of 4% hydrogen in air, the stack reaches its end of life (EOL). Alternatively, a low resistive point between the anode and cathode results in current flow through the contact point and local heat generation. This could burn the membrane and result in EOL of the fuel cell stack. A diagnostic technique is proposed to detect cells in which membrane pinholes or electric short occur. The technique allows both failure mechanisms to be isolated by means of a straightforward algorithm. The detection of the failure can be used as a pass/fail criterion during fuel cell stack manufacturing, whereas the isolation of the failure modes can be used to inform suitable repair procedures to be performed on the failed stacks.

Keywords: polymer electrolyte fuel cell; diagnostic; electric short; pinhole; hydrogen crossover; quality control

* Corresponding author. Email: amniroum@sfu.ca

1. Introduction

Polymer electrolyte fuel cell (PEFC) technology is poised to expand into the transportation market. Several automotive original equipment manufacturers (OEMs) have started selling small fleets; others have plans to do so in the near future. Fuel cell busses are being deployed in several markets, including China. Fuel cell trucks, trains, and marine vessels are also all under major development. Fuel cells have also been established as a commercially viable solution for the materials handling market during the past decade. These developments are also reflected in the growing demand for reliable and accurate diagnostic tools that are needed for ramping up fuel cell manufacturing. These diagnostic tools should be able to detect and isolate manufacturing defects in the production line. This includes quality control (QC) of individual components as well as the assembled fuel cell stack. In the first two parts of this paper series, we introduced two diagnostic tools that can be used to quantify hydrogen transfer leak for R&D and operational applications in PEM fuel cells [1,2]. In the present work, we introduce a diagnostic tool that can be used to detect and isolate hydrogen transfer leak resulting from membrane pinhole or electric short during the manufacturing of PEFC stacks.

Two of the main beginning of life (BoL) manufacturing defects that cause early failure of fuel cell stacks are membrane pinholes and electric shorts in the cell. Membrane pinholes are formed during membrane production or at various stages during fabrication of the membrane electrode assemblies (MEAs) or stack, e.g. through puncturing. They result in gas crossover which inhibits one of the primary functions of the membrane that is separating anode and cathode reactants [3]. With a cathode overpressure, i.e., cathode pressure higher than anode, air would flow through the pinholes from cathode to anode. As the pinholes get larger, so does the flow of air through them, up to a point that the crossover oxygen would consume all the hydrogen in the anode, resulting in hydrogen starvation. This in turn could result in cell reversal, burn in the membrane and end of life (EOL) of the fuel cell [4-7]. As a precaution, fuel cells are typically operated with an anode overpressure, as

oxygen starvation is less critical when compared to hydrogen starvation [5-8]. Under such conditions, membrane pinholes lead to hydrogen crossover from anode to cathode, resulting in hydrogen oxidation reaction (HOR) at the CCL. The local heat generated as a result of the HOR can exacerbate the growth of pinholes and further increase hydrogen crossover. As the size of the pinholes grows, so does the rate of hydrogen crossover, where it reaches a limit that it can consume all the oxygen in the cathode and exit the fuel cell as hydrogen emission. The lower explosion limit (LEL) for hydrogen combustion in air is 4%. In order to ensure safety, the admissible hydrogen concentration emission is typically set at 2%. Once hydrogen emission from the cathode passes this 2% limit, the stack must be shut down. The above processes have negative effects on performance, fuel utilization, and lifetime of the PEFC stack. In order to mitigate them, it is essential to ensure pinholes do not exist in manufactured fuel cell stacks.

Electric shorts can also occur due to various manufacturing defects, e.g., edge connection occurring between the bipolar plates, especially when using thin metallic bipolar plates that can bend easily [9]. An electric short current result in electron transfer from anode to cathode, where these electrons participate in oxygen reduction reaction (ORR) without having performed external work, reducing PEFC efficiency and fuel utilization. Furthermore, the localized heat generated due to electric short can burn the membrane and result in EOL during membrane break in. As such, it is essential to detect electric shorts in the QC stage of PEFC stack manufacturing process.

Membrane pinholes and electric short defects are similar in the sense that result in hydrogen transfer leak and reduced hydrogen utilization, mixed potential at the cathode catalyst layer (CCL), and prematurely precipitate the end EOL of the stack. However, they require different actions in order to repair the affected PEFC stack. MEAs with pinhole need to be replaced by new ones that do not have a convective path for gasses, whereas electric short is primarily a bipolar plate effect and requires their replacement. As such, it is desired to separate the two failure modes

during QC to allow for suitable repair mechanism to be performed once the fuel cell stack.

One method for detecting a cell with low electric resistance is to apply a small potential across the anode and cathode using a potentiostat and measure the resulting current. If there is electric short in the cell, the applied potential would result in a significant current. This method is very simple and can rapidly identify and quantify the size of the electric short, however, it is not suitable for detecting electric shorts in a fuel cell stack. This is because the cell voltage monitoring (CVM) system can only measure individual cell potentials and is not suitable for conducting large current given the small size of contact probes. Note that when using a potentiostat, the current setting needs to be limited to ensure that small resistances do not result in high currents, which would lead to burning the membrane.

In [10], the authors suggested supplying hydrogen and nitrogen and performing linear sweep voltammetry (LSV) to detect short resistance from the slope of the I-V curve. Authors in [11, 12] suggested using LSV to quantify the hydrogen transfer leak in the membrane using a cell potential ~400 mV. Under these conditions, the current is consumed to oxidize the crossover hydrogen and can be used to quantify the leak using Faraday's law. While LSV is a very accurate method for detecting these processes, it is not suitable for manufacturing applications as it cannot be applied to fuel cell stacks. This is due to the fact that similar to potentiostatic measurements, LSV also requires potential control and current supply, which is not feasible with CVM connections.

Authors in [13,14] use a passive electrical measurement method to detect pinholes and electric leaks in the fuel cell stack. In this method the fuel cell is humidified with air and the double layer capacitances at the anode and cathode electrodes are charged with a small dc current up to 0.45 V. the current source is then disconnected and the rate of voltage drop is used to detect electric short or pinholes in the membrane. This technique is suitable for detecting pinholes and electric

shorts in fuel cell stacks; however, it cannot be used to separate the two failure modes.

In order to ensure that a fuel cell is free of hydrogen crossover leaks, an internal leak check is performed after stack assembly. This is done by pressurizing anode or cathode of the fuel cell stack with air and examining the opposite manifold for airflow [1]. If there is any air flowing out of the opposite electrode, it means that a convective path exists between anode and cathode, which could be an indication of a pinhole in one or few of the membranes. One challenge with this method is that it is desirable to detect very small leak rates in a manufactured stack in order to detect possible pinholes in the membrane, e.g., smaller than 1 sccm/cell. However, a large automotive stack has a large dead volume in the flow fields and manifolds. As such, a small change in operating conditions such as pressure and/or temperature could result in a false alarm in the downstream mass flow meter that measures the flow rate at the stack exhaust. Therefore, this method tends to be slow to ensure steady state conditions have reached, and it is poor in terms of repeatability and reproducibility. Furthermore, even when a leak is detected using this method, it cannot identify the leaky cell, so that proper repair procedures cannot be performed.

Authors in [15, 16] applied hydrogen and air with a small anode overpressure and measured the open circuit voltage (OCV) to detect pinholes in the membrane. If a pinhole exists in the membrane, hydrogen would crossover through the pinhole, combine with oxygen, and result in a mixed potential in the cathode. Therefore, the leaky cell will have a lower OCV compared to normal cells. This method is very sensitive for detecting pinholes in the membrane. However, the limitation of the method for manufacturing applications is that if electric short exists in the stack, it is not safe to supply reactants to the fuel cell. Supplying hydrogen and air would result in ~1 V potential across each cell, which would result in localized current passing through the short contact, resulting in local heat generation, burn in the membrane, and a so-called rapid oxidation event (ROE) in the presence of hydrogen and oxygen.

Authors in [17-19] suggested using the rate of the voltage drop after stopping the supply of hydrogen and air to detect pinholes in the membrane, which has similar safety problems if there is electric short in the membrane, as it could cause burning of the membrane and ROE.

In [1], authors proposed supplying hydrogen and nitrogen to the anode and cathode of a fuel cell, respectively, and measuring the OCV to determine the flow rate of hydrogen transfer leak. They showed that the method is accurate when the flow rate of hydrogen transfer leak is larger than hydrogen permeation through the membrane. They also showed that the flow rate of hydrogen transfer leak is proportional to the pressure difference between anode and cathode. However, the method has limitations when the hydrogen transfer leak flow rate is smaller than the permeation rate.

In this paper, we introduce a diagnostic tool that allows electric shorts and membrane pinholes in individual cells of a PEM fuel cell stack to be detected and isolated using hardware that is available on standard fuel cell test stations. We first derive a simple physical model that relates cell resistance, hydrogen flow rate due to permeation through the membrane, hydrogen crossover due to gas flow through pinholes, and OCV. To discriminate the two failure modes, we show that the OCV depends on the hydrogen concentration on the anode in the case of an electric short and on the anode overpressure in the case of a pinhole. For both failure modes, the model is compared to experimental data for a single cell to demonstrate the diagnostic capability. Moreover, the diagnostic methodology is tested on a fuel cell stack with both failure modes to examine its detection and isolation capability.

2. Experimental

Testing was performed on two different cell sizes and architectures, i.e., Greenlight Innovation 50 cm^2 and PowerCell 195 cm^2 hardware. An ND-Yag laser was used to create pinholes in the membrane. Experimental details will be explained in the following four sections.

2.1. Greenlight setup

A 50 cm^2 co-flow serpentine flow field channel was used for the single cell and short stack experiments. A Nafion 212 Membrane coated with 0.3 $mgPt/cm^2$ catalyst on both sides and Sigracet 29BC carbon paper Gas Diffusion Layer (GDL) was used. The operating conditions used for these experiments are shown in Table 1, unless specified otherwise.

A Greenlight Innovation G100 test station was used for the single cell testing. The anode and cathode have a 1 and 2 NLPM hydrogen and air mass flow controllers (MFCs), respectively, along with 2 NLPM nitrogen MFCs on both electrodes. The nitrogen MFC allows for mixing gasses and reducing the reactant supply concentration as desired. Contact humidifiers were used to control the humidity on both electrodes and heated deionized water was circulated in the cell to control the stack temperature. The anode flow subsystem has a three-way bypass valve before the humidifier (Fig. 1). Due to the large volume of the humidifier, changes in concentration take a long time to settle to a new steady state at the cell level. This bypass valve allows rapid change of reactant concentration, for the cost of supplying the cell with dry gas. As shown later on this work, the proposed diagnostic tool is not sensitive to humidification levels; however, rapid testing is essential for manufacturing applications. Gamry, Reference 3000 Impedance Analyzer was used to conduct LSV.

2.2. PowerCell setup

For stack experiments, a 10-cell stack with an active area of 195 cm^2 was used. Greenlight Innovation G200 test station was used for testing. The anode has 80 NLPM hydrogen and 35 NLPM nitrogen MFC with gas mixing capability. The cathode has a 200 NLPM air and Nitrogen MFC. The stack was mounted in counter flow configuration, temperature and humidity set points was set as in Table 1, unless mentioned otherwise.

2.3. Electric short

An electric short between the anode and cathode was simulated by connecting a known resistance between the bipolar plates. This resistance would create a known conductive path between the two electrodes and path for electron conduction. By changing the value of the resistance, different electric short resistances were simulated.

2.4 Pinhole formation

In order to create pinholes at controlled locations in the MEA, A 100 W ND-Yag laser was used. Experiments were carried with different number of laser pulses to modulate the size of the pinhole. Pinhole size characterization was performed by stripping the GDL and catalyst layer, followed by measuring the size of the pinhole in the membrane. The result of this experiment is shown in Fig. 2. It can be seen that there is a linear relationship between the number of laser pulses and the size of the pinhole. For the test, 200 laser pulses were used.

3. Results and discussions

When hydrogen and air are supplied to the anode and cathode of a PEM fuel cell, it results in an OCV of around ~1 V between the two electrodes and respective bipolar plates. If an electric short or low resistance point exist between the electrodes or the bipolar plates, current will pass through it. The magnitude of this current depends on the conductance of the electric short. This current is a parasitic loss and will reduce the voltage and power performance of the fuel cell. In addition, as the current passes through the small surface area of the electric short, it results in a hot spot at the contact point. If the conductance of the electric short is relatively high, the generated heat could burn the MEA and fail the fuel cell stack. In order to mitigate from such event, it is desirable to reduce the cell potential during electric leak testing, so that the current is smaller, and less heat is produced. It is also desirable to use an inert gas on the cathode side to reduce the possibility of ROE, in case the electric leak results in melting and transfer leak in the membrane. As such, we propose developing a method that uses hydrogen and nitrogen on the anode and

cathode sides of the fuel cell. This would reduce the OCV by an order of magnitude and would eliminate oxygen from the testing procedure.

3.1. Model-based Description

With hydrogen and nitrogen are supplied at anode and cathode of the PEFC, hydrogen permeates from anode to cathode due to concentration gradient across the membrane. The fuel cell potential, based on Nernst equation, is

$$E = -\frac{RT}{2F} ln \frac{P_{H2,c}}{P_{H2,a}}, \qquad (1)$$

where E is the OCV, R the ideal gas constant, T the cell temperature, F the Faraday constant, $P_{H2,c}$ the partial pressure of hydrogen in the cathode, and $P_{H2,a}$ the partial pressure of hydrogen in the anode. The partial pressure of hydrogen in the anode can be calculated from the total anode pressure, P_a, partial pressure of vapor in the anode, $P_{w,a}$, and mole fraction of hydrogen in the anode stream, x,

$$P_{H2,a} = x\left(P_a - P_{w,a}\right). \qquad (2)$$

The rate of hydrogen transfer leak across the membrane depends on the rates of three processes: rate of hydrogen permeation through the membrane, Q_D, rate of hydrogen crossover through the pinhole, Q_{H2}, and rate of hydrogen production on the cathode due to short, Q_S, as illustrated in Fig. 3. Note that in Fig. 3, the diffusion media between MEA and anode/cathode plates are not shown for simplicity. These diffusion media are also the electric conductive path that allows electrons to reach the reaction sites at the CCL and combine with protons that are conducted through the membrane to produce hydrogen.

The partial pressure of hydrogen on the cathode depends on the rate of hydrogen transfer via permeation through the leak in the membrane, crossover through pinholes, and production due to short, as well as the flow of nitrogen in the cathode, Q_{N2}, total gas crossover across the pinhole, Q_L, and the total cathode pressure, P_c,

$$P_{H2,c} = \frac{Q_D + Q_S + Q_{H2}}{Q_{N2} + Q_D + Q_S + Q_L} P_c. \qquad (3)$$

Note that the total gas crossover across the pinhole, Q_L, is different than hydrogen crossover, Q_{H2}, as the anode gas can contains water vapor and possibly nitrogen in addition to hydrogen. The diagnostic tool can be designed such that the nitrogen flow rate in the cathode (Q_{N2}), is significantly higher than the gas crossover from anode to cathode due to permeation, (Q_D), electric short (Q_S), and leak (Q_L). Under such conditions, Eq. 3 simplifies to

$$P_{H2,c} \approx \frac{Q_D + Q_S + Q_{H2}}{Q_{N2}} P_c . \qquad (4)$$

Based on Fick's law, hydrogen permeation through the membrane can be written as

$$Q_D = AK_{H2} \frac{P_{H2,a} - P_{H2,c}}{d} \qquad (5)$$

where A is the active geometric area of the cell, K_{H2} membrane permeability, and d membrane thickness. Since a high rate of nitrogen flow is used on the cathode side, the partial pressure of hydrogen in the cathode is significantly lower than that in the anode, simplifying Eq. 5 to

$$Q_D \approx AK_{H2} \frac{P_{H2,a}}{d} \qquad (6)$$

The rate of hydrogen production at the cathode due to electric short can be calculated from the short current, i_s, using Faraday law. This current is equal to the cell potential, E, over the short resistance, R_s, giving

$$Q_S = \frac{i_s}{2F} = \frac{E}{2FR_s}. \qquad (7)$$

The rate of gas crossover across the pinhole, Q_L, is directly proportional to the pressure difference across the membrane and the membrane leak size, S,

$$Q_L = S(P_a - P_c). \qquad (8)$$

The hydrogen gas crossover flow rate, Q_{H2}, can be calculated from the total crossover flow rate in Eq. 8, and the ratio of hydrogen partial pressure in the anode, $P_{H2,a}$, to the anode pressure, P_a, giving

$$Q_{H2} = \frac{P_{H2,a} S(P_a - P_c)}{P_a} . \qquad (9)$$

Substituting Eqs. 6,7,9 in Eq. 4. results in an expression for the hydrogen partial pressure in the cathode, $P_{H2,c}$, and replacing that in Eq. 1 gives

$$E \approx -\frac{RT}{2F} ln\left[\frac{P_c}{Q_{N2}}\left(\frac{AK_{H2}}{d}+\frac{E}{2FR_S P_{H2,a}}+\frac{S(P_a-P_c)}{P_a}\right)\right]. \quad (10)$$

In Eq. 10, the first term in the curved parenthesis represents hydrogen permeation through the membrane. This term does not depend on hydrogen pressure on the anode side.

The second term in curved parentheses on the right-hand side of Eq. 10 represents the electric leak. This term is inversely proportional to the partial pressure of hydrogen in the anode. Decreasing $P_{H2,a}$ can be used to make this second term large enough so that it will be significant in comparison to the first term, such that the OCV in a cell with a given electric short is detectable from one that does not have such conductive path. This is specifically important when one must test a fuel cell stack with a large surface area and/or small membrane thickness, and is interested in detecting a large contact resistance, e.g., between touching bipolar plates.

The third term on the right-hand side of Eq. 3 represents the effect on the cell potential due to the impact of a hydrogen crossover leak through a pinhole. This term depends on the ratio of cathode to anode pressure. Assuming a fixed cathode pressure, a variation of the anode pressure will change the importance of this term relative to the other two contributions. The case with no pinhole in the membrane corresponds to zero leak rate and thus vanishing effect of this term on cell potential, regardless of the difference between the anode and cathode pressures. However, when a pinhole exists in the membrane and the leak rate is small, an increase in the anode pressure would amplify the effect of this term, making the pinhole detectable.

The above analysis suggests that a drop in the individual cell OCV can be used to detect pinholes and electric shorts. Furthermore, the two failure modes can be isolated by changing the anode pressure and concentration, i.e., an increase in anode pressure would drop the OCV of cells with pinhole, whereas the drop in hydrogen concentration will make cells with internal short to become evident. These are illustrated in the following sections.

3.2. Pinhole detection

The relationship between the hydrogen crossover leak rate and overpressure was validated for inlet and outlet pinholes. An ND-Yag laser was used to create a pinhole at one end of the MEA as explained in section 2.4. The MEA was then placed in the single cell hardware. Two experiments were conducted between which the flow directions of hydrogen and nitrogen gases were changed between inlet and outlet. This resulted for the pinhole location to be at the beginning and end of the flow field. For each case, the OCV was recorded and LSV was conducted. The hydrogen crossover rate was calculated from the observed OCV using the Nernst equation (Eq. 10 and then Eq. 9). For comparison, the hydrogen crossover flow rate was also calculated from the LSV measurement using the Faradic relationship explained in [1, 11, 12]. In this method, the cell current at a potential of ~400 is consumed to oxidize the hydrogen that crosses over from anode to cathode, and the Faraday law is used to calculate the rate of hydrogen crossover rate based on the measured current. The corresponding hydrogen crossover leak flow rates using the Nernst and Faradaic methods are shown in Fig. 4.

It can be seen in Fig. 4 that when the pinhole is at the cell inlet, both the Faradaic current and Nernst potential are in good agreement with respect to the leak rate. However, when the pinhole is moved to the outlet, both methods underestimate the leak. The value predicted by the Nernst potential is higher than the Faradaic estimation. The reduction in the Faradaic estimation can be due to the fact that when a pinhole is located close to the outlet, some of the hydrogen can leave the cell before it participates in the Faradaic reaction, therefore reducing the leak rate estimation. Furthermore, a leak at the outlet would only affect the downstream cell potential as the upstream hydrogen concentration is not changed. This causes a mixed potential along the flow field plate which results in an underestimation of the leak rate using the Nernst potential. However, in all cases, linear relationships were observed between anode overpressure and estimated leak rate. This suggests that

an increase in overpressure can be used to detect and isolate leaks from background permeation.

In order to calibrate the technique for the overpressure that is required to detect small pinholes, let's denote E_1 as the cell potential for a cell without electric short or pinholes (second and third terms in the *ln* parenthesis in Eq. 10 will be eliminated), and E_2 as the cell potential for a cell with a pinholes (only second terms in the *ln* parenthesis in Eq. 10 will be eliminated). The potential drop, $\Delta E = E_2 - E_1$, will be given by

$$\Delta E = -\frac{RT}{2F} ln\left(1 + \frac{Sd}{AK_{H2}P_a}(P_a - P_c)\right). \qquad (11)$$

From Eq. 11, the required overpressure, $\Delta P = P_a - P_c$, can be derived from the potential drop, permeation, and leak rates as:

$$\Delta P = \frac{AK_{H2}P_a}{dS}\left(e^{-\frac{2F\Delta E}{RT}} - 1\right). \qquad (12)$$

The permeation current density measured using LSV for Nafion 112 membrane at 25 ˚C and 100 kPa is 0.5 mA/cm^2 and 2 mA/cm^2 at 80 ˚C and 100 kPa, resulting in an effective permeation rate (K_{H2}/d) of 3.5×10^{-5} and 1.4×10^{-4} sccm/kPa, respectively. Given calibration and fuel cell voltage deviations, a 10mV voltage drop would be large enough to reliably detect hydrogen crossover. For a small hydrogen crossover of 0.05 sccm/kPa, the overpressure required to achieve such a voltage drop is graphed in Fig. 5 as a function of cell area using Eq. 12.

It can be seen in Fig. 5 that the overpressure required to detect a leak increases linearly with cell active surface area. This is expected as the increase in surface area linearly increases the total hydrogen permeation flow rate through the membrane. As the drop in cell potential is determined by the hydrogen concentration in the cathode, the hydrogen crossover rate must be increased proportionally with the hydrogen permeation flow rate to result in the same change in cathode hydrogen concentration. This will require a proportionally higher overpressure, and thus the

relation between the required overpressure and the cell active surface area is linear as well.

It is also seen is Fig. 5 that higher temperatures require a higher overpressure for leak detection, which is due to the increased permeation rate at elevated temperatures. This suggest that lower temperatures are more suitable for leak detection. This is also desired from a manufacturing perspective, as room temperature allows for faster testing. Furthermore, the range of overpressures shown in Fig. 5 suggests that an overpressure of 20 kPa is high enough to detect pinholes for a 50 cm^2 cell, which is the value we adopt for this study.

To examine the detectability of pinholes in PEFC stacks using change in anode overpressure, a 2-cell short stack was built using the Greenlight cell architecture described in section 2.1 and operating conditions of table 1. An intact MEAs and an MEA with pinhole in the middle and end of the cell was used. The pinholes were constructed using the ND-Yag laser explained in section 2.4. The stack was operated at zero and 20 kPa anode overpressure. The result of the experiment is shown in Table 2. It can be seen that an increase in anode overpressure results in a voltage drop in cell 2 with pinholes, however, does not affect the intact membrane. This illustrates that an increase in anode overpressure can be used to detect cells with pinhole in a fuel cell stack.

3.3. Electric short detection

To examine the accuracy of the model presented in Eq. 10, the MEA described in section 2.1 was operated with the conditions mentioned in Table 1. Different resistances were added parallel to the bipolar plates to simulate an electric short and the cell potential was measured. The cell potential with no electric short was used to calculate the permeation term in Eq. 10 (first term in parenthesis). This value was then used to calculate the cell potential for the subsequently tested resistances. The measured and calculated cell potentials are shown in Fig. 6.

It can be seen in Fig. 6 that the cell potential calculated by the model is in good agreement with the experimental data. It can also be seen that the change in cell potential is relatively small when adding a 10 Ω resistor, whereas this change gets larger with smaller resistance. This shows the limitation for detecting a short that has a large resistance with pure hydrogen. However, hydrogen partial pressure can be adjusted to detect a specified electric resistance, as discussed below.

The relative size of the electric short compared to hydrogen permeation through the membrane can affect the detectability of hydrogen production due to electric short versus the background hydrogen permeation flow rate. However, it can be seen in Eq. 10 that while reduction in hydrogen concentration does not affect cell potential as a result of permeation (first term in parenthesis), it can magnify the effect of hydrogen production due to electric short (second term in parenthesis). As such, the hydrogen concentration can be calibrated such that the short resistance of interest be detected for a given MEA, cell architecture, and active area. To illustrate this, three resistance values of 10 Ω, 1 Ω, and 0.1 Ω were connected in parallel to the single cell described in section 2 to simulate a short resistance. The hydrogen molar fraction was then reduced, and the result of this experiment is shown in Fig. 7.

It can be seen in Fig. 7 that as the electric short resistance reduces, changes in hydrogen molar fraction has a more pronounced effect on OCV, illustrated by the slope of the curves. The dashed line in Fig. 6 illustrates the point at which OCV drops 15% below its value at 100% hydrogen molar fraction. It can be seen that this drop occurs at about 5% hydrogen concentration for the 10 Ω resistance, at 20% hydrogen molar fraction for 1 Ω resistance, and at 50% hydrogen molar fraction for 0.1 Ω resistance. This illustrates that the diagnostic methodology can be calibrated to detect different electric shorts based on adjusting the molar fraction of hydrogen during QC.

The hydrogen molar fraction can be changed by adding nitrogen to the hydrogen stream. However, the changes in hydrogen molar fraction can be relatively slow

when using a contact humidifier. This is due to the large volume of the humidifier and the dilution of the mixed hydrogen/nitrogen stream with the existing hydrogen in the humidifier. Given that the electric short detection method is designed for QC, it is essential to detect failures in a timely manner. For this purpose, a three-way bypass valve is added that allows bypassing the humidifier (Fig. 1). In this configuration, changes in gas ratio will result in a timely change in the cell potential, whereas the downside of this approach is that it does not allow for the gasses to be humidified. However, given that only changes in cell potential are required to detect an electric short, it is feasible to measure the cell potential without humidifying the cell. To illustrate this, the Greenlight cell architecture of section 2.1 and operating conditions of the short stack in table 1 were used, i.e., ambient temperature for cell and humidifier. A 1 Ω resistor was then added to the bipolar plates to simulate an electric short. The hydrogen molar fraction was then changed under two scenarios: with anode humidifier in the loop and with anode humidifier bypassed using the three-way valve shown in Fig. 1. The result of this experiment is shown in Fig. 8, where the incident time of the three experiments is normalized to zero.

It can be seen in Fig. 8 that adding the 1 Ω resistance results in an immediate drop in OCV; it takes about 10 seconds for the cell potential to reach the new steady state (solid grey line). This amount corresponds to the time required for the cathode hydrogen concentration to reach the new steady state involving the production of hydrogen on the cathode side when the resistor is added. With the 1 Ω resistor connected, the anode hydrogen molar fraction was then changed from 100% to 10% (black dashed line). It can be seen that it takes a about 150 seconds for the cell potential to reach equilibrium, which corresponds to the dilution of the gas stream in the humidifier. In the next experiment, the hydrogen molar fraction in the anode gas mixture was changed with the humidifier bypassed (blue dotted line). It can be seen that the OCV reached the new steady state much faster, in less than 20 seconds. This illustrates that bypassing the humidifier can be used to expedite the electric short detection procedure.

In Fig 8, the initial OCV is lower when the humidifier is bypassed compared to the humidified scenario. Although the humidifier is at ambient temperature, it still increases the dry gas water content when the gasses move through it, thereby increasing the OCV. However, the drop in OCV with and without humidifier is similar and around 200 mV. This illustrates that bypassing the humidifier does not impede the detection capability of the method, as the voltage drop is the measure that is used for detecting electric shorts.

Table 3 shows the result of electric leak test on a 10 cell PowerCell stack explained in section 2.2 prior to membrane break-in. It can be seen in row 1 that potentials at all cell individual cells in the stack are within a 2mV range when all cells are healthy. The second row shows the cell potentials when a 10 Ω resistance was added to cell #8. This resistance is not detectable under these conditions, as the potential of cell #8 does not show a significant change. The third row shows the cell potential when a 0.8 Ω resistance is added to cell #4. In this case, the potential of cell #4 drops by 6 mV, rendering the defect detectable, whereas other cell potentials do not change. By looking at the third row alone it is possible to identify cell #4 as having an electric short, whereas this is not detectable for cell #8. Next, adding another 0.1 Ω resistance to cell #1 results in a 12 mV drop in cell potential as seen in row 4. Row 5 shows the cell potentials with the same electric leak defects added to cells #1, #4, and #8, but for hydrogen molar fraction was reduced to 10%. With the reduced hydrogen molar fraction to 10%, all defects are found above the detection limit, including the 10 Ω resistance on cell #8, as they all deviate by more than Delta E = 5 mV from the potential of defect-free cells. This suggests that using a low hydrogen molar fraction that has been calibrated for the size of short resistance that needs to be detected, it is possible to detect cells with electric short by a single measurement using lower cell potential as detection criteria.

Note that larger resistances become more difficult to detect and less problematic in terms of failures. While the required isolation between the plates depends on stack specifications and not straightforward to calculate or measure, a 0.1 W power

dissipation is believed to be small and safe enough. This in turn translates into a 10 Ω resistance, given the maximal voltage of 1 V that each cell experiences. As such, the tests in this work have been conducted to detect a short resistance as large as 10 Ω.

3.4. Gas crossover and electric leak isolation

To examine the combined impact of pinhole and electric short in a fuel cell stack, a 3-cell short stack was constructed using the Greenlight cell architecture in section 2. A brand new MEA was used for cell 1, a previously conditioned MEA was used for cell 2, and an MEA with pinhole in the middle and end of the cell was used for cell 3. A 10 Ω resistance was placed in parallel with cell 1 to simulate an electric short. All MEAs were dry and the bypass valve in Fig. 1 was used to avoid humidification. The stack was operated at zero and 20 kPa overpressure and 10% hydrogen molar fraction. The result of the test is shown in table 4.

It can be seen in table 4 that with 100% hydrogen and no over pressure, cell 1 and 2 have similar potential, whereas the potential of cell 3 is lower. This suggest that cell 3 has a defect but cannot distinguish between the possibility of a pinhole or a low resistive path. When the hydrogen pressure is increased to impose a 20 kPa overpressure on the cell, the potential of cell 3 drops significantly, whereas the potential of cells 1 and 2 do not change. This suggests that the failure mode of cell 3 is hydrogen crossover through membrane pinholes. Finally, with a drop in the molar fraction of hydrogen to 10%, the potential of cell 1 also drops, revealing a short resistance between the electrodes. This experiment illustrates that changing the hydrogen pressure and molar fraction can be used to detect and isolate membrane pinholes and electric short in PEFC stacks. Furthermore, it shows that the failure modes can be detected and isolated without the need to humidify the membrane, which makes this method suitable for rapid QC during the manufacturing processes.

4. Conclusions

The article proposed a diagnostic method for in-situ detection and isolation of membrane pinholes and electric shorts in polymer electrolyte fuel cell stacks. The method uses the effect of pressure difference between anode and cathode and the hydrogen partial pressure in the anode as two independently controllable parameters to discriminate between the two failure modes. An analytical model was developed to capture and quantitatively characterize the effects of electric short and hydrogen crossover leak on cell potential. The model showed that reducing the hydrogen partial pressure in the anode amplifies the voltage loss caused by an electric short in a cell; whereas increasing the pressure difference between anode and cathode increases the effect of hydrogen crossover on the cell voltage drop. The sensitivities of the two failure modes to different operating parameters can be used to identify cells with pinhole and electric short in a fuel cell stack. The diagnostic tool can be applied as a means of quality control of fuel cell stack manufacturing; it is suitable to screen stack for defects of its individual cells prior to membrane break-in and stack operation. Furthermore, it uses individual cell potential for the detection of faulty cells, which is readily available on fuel cell test stations.

Acknowledgement

Authors would like to acknowledge 4D Labs at Simon Fraser University for providing support using the Nd-YAG laser. Funding for this project was provided by NSERC CRD [grant number CRDPJ 513543-17]. Authors also want to acknowledge Qingxin Zhang, Amin Noori, and Carlie Olfert for their contributions to the experimental work in this paper.

References

[1] A. M. Niroumand, O. Pooyanfar, N. Macauley, J. DeVaal, and F. Golnaraghi, J. Power Sources 278 (2015) 652-9.

[2] A. M. Niroumand, H. Homayouni, J. DeVaal, F. Golnaraghi, and E. Kjeang, J. Power Sources 322 (2016) 147-54.

[3] W. Lu, Z. Liu, C. Wang, Z. Mao, and M. Zhang, Int. J. Energy Res. 35 (2011) 24-30.

[4] S.D. Knights, K.M. Colbow, J. St-Pierre, and D.P. Wilkinson, J. Power Sources 127 (2004) 127-34.

[5] A. Taniguchi, T. Akita, K. Yasuda, and Y. Miyazaki, J. Power Sources 130 (2004) 42-9.

[6] Y.Z. Liu, B.K. Brady, R.N. Carter, B. Litteer, M. Budinski, J.K. Hyun, and D. A. Muller, J. Electrochem. Soc. 155 (2008) B979-84.

[7] N. Yousfi-Steiner, Ph. Moc¸otéguy, D. Candusso, D. Hissel, J. Power Sources 194 (2009) 130–145.

[8] M. Gerard, J.P. Poirot-Crouvezier, D. Hissel, M.C. Pera, Int. J. Hydrogen Energy 35 (2010) 12295-307.

[9] F. Barbir, PEM Fuel Cells (second edition), Academic Press (2013).

[10] M. V. Williams, H. R. Kunz, and J. M. Fenton, J. Electrochem. Soc. 152 (2005) A635-44.

[11] S. Nakamura, E. Kashiwa, H. Sasou, S. Hariyama, T. Aoki, Y. Ogami, and H. Nishikawa, Electrical Engineering in Japan 174 (2011) 1-9.

[12] M. Inaba, T. Kinumoto, M. Kiriake, R. Umebayashi, A. Tasaka, and Z. Ogumi, Electrochim. Acta 51 (2006) 5746-53.

[13] L. Flandin, A.S. Danerol, C. Bas, E. Claude, G. De-Moor, and N. Alberola, J. Electrochem. Soc. 156 (2009) B1117-23.

[14] G. De-Moor, N. Charvin, C. Bas, N. Caque, E. Rossinot, and N. Flandin, IEEE Trans. Ind. Electron. 62 (2015) 5275-82.

[15] B. Sompallli, B.A. Litteer, W. Gu, and H.A. Gasteiger, J. Electrochem. Soc. 154 (2007) B1349-57.

[16] C. Lim, L. Ghassemzadeh, F. Van Hove, M. Lauritzen, J. Kolodziej, G.G. Wang, S. Holdcroft, and E. Kjeang, J. Power Sources 257 (2014) 102-10.

[17] G. Tian, S. Wasterlain, I. Endichi, D. Candusso, F. Harel, X. Francios, et al., J. Power Sources 182 (2008) 449-61.

[18] G. Tian, S. Wasterlain, D. Candusso, F. Harel, X. Francios, D. Hissel, and X. Francios, Int. J. Hydrogen Energy 35 (2010) 2772-6.

[19] M.R. Ashraf Khorasani, S. Asghari, A. Mokmeli, M.H. Shahsamandi, and B. FaghihImani, Int. J. Hydrogen Energy 35 (2010) 9269-75.

[20] S.S. Kocha, J.D. Yang, and J.S. Yi, AIChE J. 52 (20060 1916-25.

Figures

Fig. 1

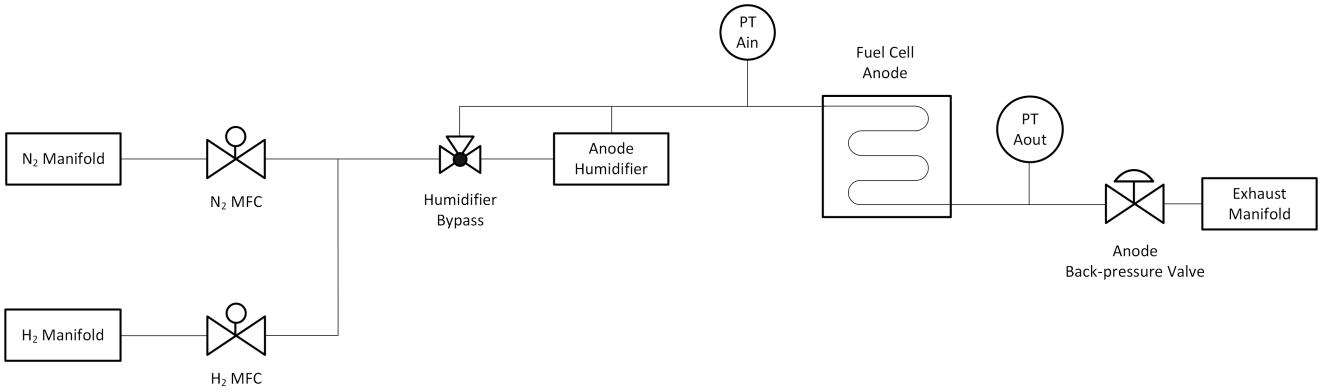

Fig. 2

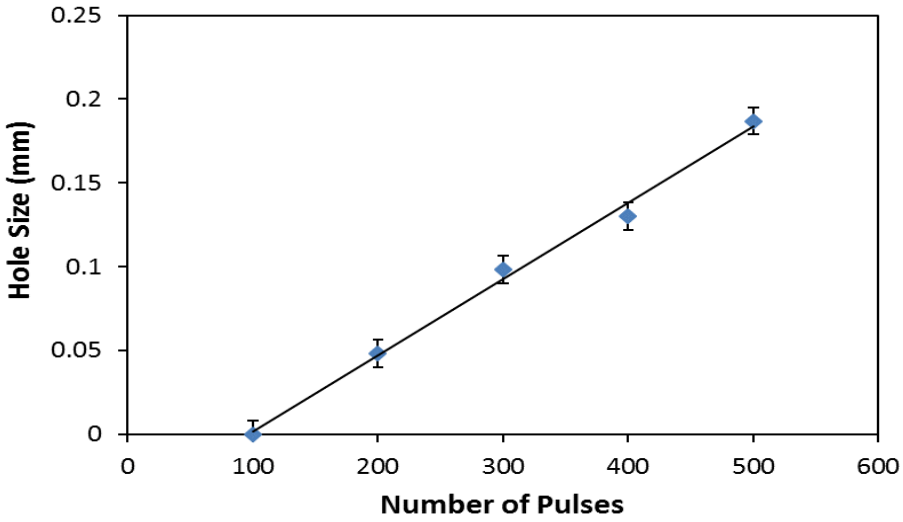
0.25
0.2
0.15
0.1
0.05
0
Hole Size (mm)
0
100
200
300
400
500
600
Number of Pulses

Fig. 3

Fig. 4

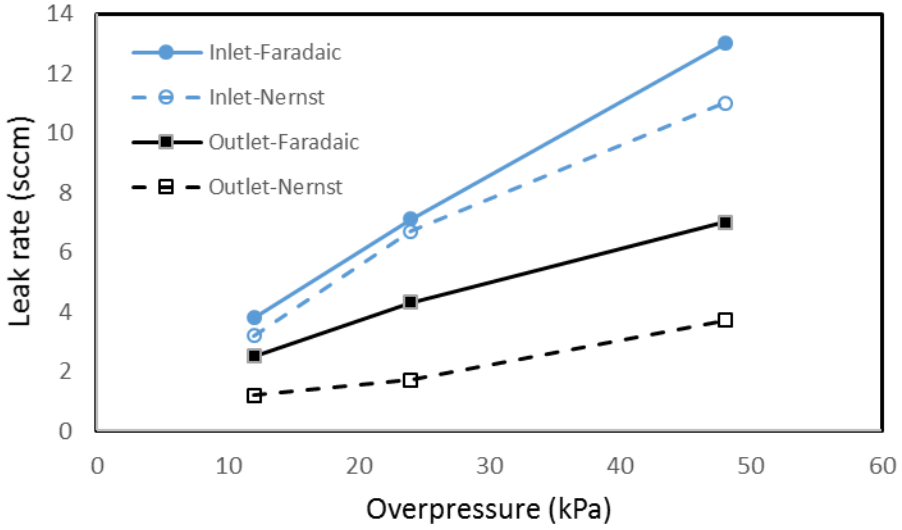
Leak rate (sccm)
Overpressure (kPa)
Inlet-Faradaic
Inlet-Nernst
Outlet-Faradaic
Outlet-Nernst
0
2
4
6
8
10
12
14
0
10
20
30
40
50
60

Fig. 5

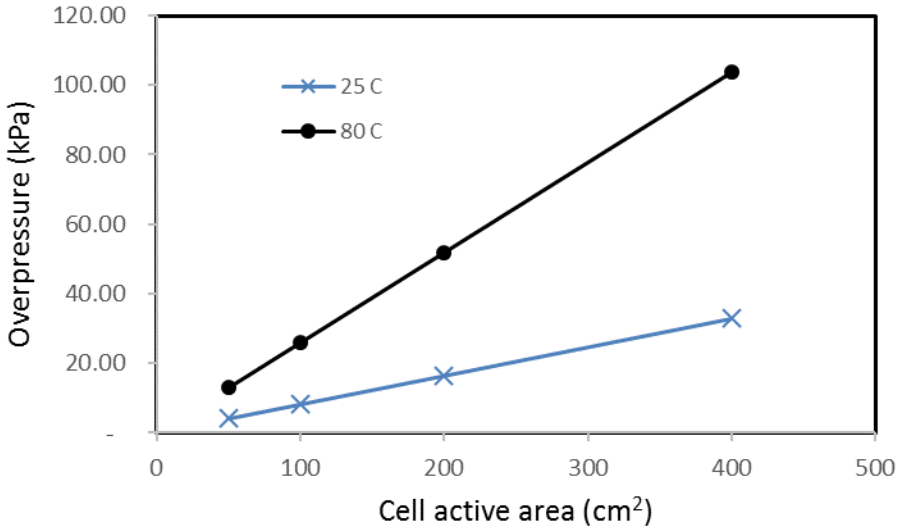
120.00
100.00
80.00
60.00
40.00
20.00
-
Overpressure (kPa)
25 C
80 C
0
100
200
300
400
500
Cell active area (cm2)

Fig. 6

Fig. 7

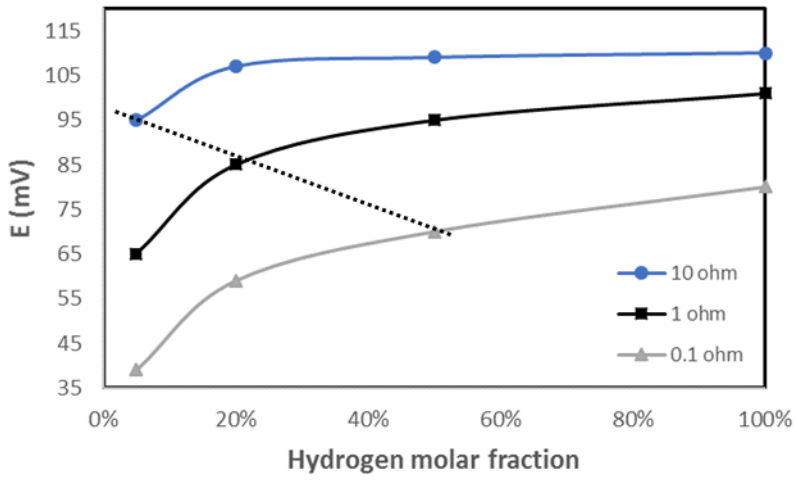
115
105
95
85
75
65
55
45
35
E (mV)
0%
20%
40%
60%
80%
100%
Hydrogen molar fraction
10 ohm
1 ohm
0.1 ohm

Fig. 8

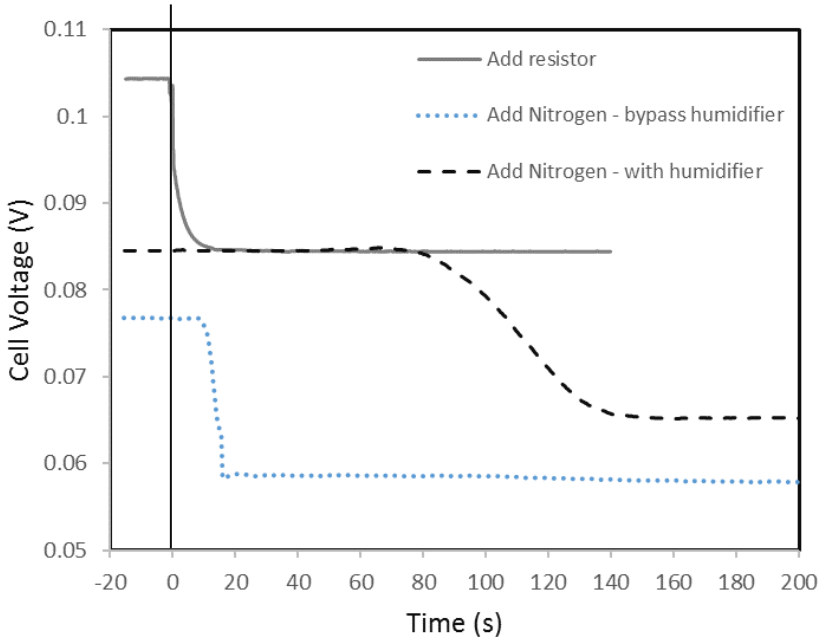
0.11
0.1
0.09
0.08
0.07
0.06
0.05
Cell Voltage (V)
-20
0
20
40
60
80
100
120
140
160
180
200
Time (s)
Add resistor
Add Nitrogen - bypass humidifier
Add Nitrogen - with humidifier

Figure captions

Fig. 1. Schematic of the test bench used.

Fig. 2. Pinhole size measured using optical microscope versus number of ND-Yag laser pulses.

Fig. 3. Schematic illustration of hydrogen transfer leak processes: hydrogen permeation rate through the membrane, Q_D, hydrogen crossover rate through the pinhole, Q_{H2}, and hydrogen production rate on the cathode, Q_S, resulting from short resistance R_S. Note that the diffusion media between the MEA and anode/cathode plates is not shown for simplicity.

Fig. 4. Hydrogen transfer leak rate measured for a pinhole at both inlet and outlet of the cell using Nernst (voltage) and Faradaic (current) methods. Single cell architecture as explained in section 2.

Fig. 5. Overpressure at which the cell voltage drops 15 mV for different cell active surface areas and temperatures. The cell cathode pressure is 100 kPag.

Fig. 6. Measured and calculated OCV at different electric short resistances for the single cell architecture explained in section 2.

Fig. 7. OCV at different hydrogen concentrations with 10, 1, and 0.1 Ω electric resistances. The dashed line illustrates when OCV drops ~15% from its value at 100% hydrogen concentration. Experiment for the single cell architecture described in section 2.

Fig. 8. Change in OCV with 1 Ω resistor added (solid gray), hydrogen molar fraction changing from 100% to 10% with 1 Ω resistor and humidifier in the loop (black dash),

and hydrogen molar fraction changing from 100% to 10% with 1 Ω resistor and humidifier bypass (blue dot). The incident time is normalized to zero.

Tables

Table 1

Parameter	**Single cell**	**Full stack**	**Short stack**
Anode pressure	150 kPag	0.1 kPag	100-120 kPag
Anode temperature	75°C	30°C	ambient
Anode humidity	73°C	30°C	bypass
Anode flow rate	1 NLPM	10 NLPM	1 NLPM
Cathode pressure	150 kPag	0.1 kPag	100 kPag
Cathode temperature	75°C	30°C	Ambient
Cathode humidity	73°C	30°C	bypass
Cathode flow rate	1 NLPM	20 NLPM	1 NLPM
Cell temperature	75°C	30°C	ambient

Table 2

H2 overpressure (kPa)	**0**	**20**
Cell #1 (mV)	95	95
Cell #2 (mV)	75	49

Table 3

H2	R (Ω)	C#	C0	C1	C2	C3	C4	C5	C6	C7	C8	C9
100	-	All	93	93	92	92	92	93	93	92	91	92
100	10	C8	93	93	91	92	92	92	92	92	91	91
100	0.8	C4	93	93	91	92	86	92	93	92	91	92
100	0.1	C1	93	81	91	92	86	92	92	91	91	92
10	"	"	87	55	85	85	62	88	88	86	80	86

Table 4

H2 molar fraction	**100%**	**100%**	**10%**
H2 overpressure (kPa)	**0**	**20**	**0**
Cell #1 (mV)	96	97	76
Cell #2 (mV)	95	95	92
Cell #3 (mV)	75	49	100

Table captions

Table 1. Single cell and stack operating conditions.

Table 2. OCV for a 2-cell short stack using Greenlight cell architecture in section 2.1. A new MEA was used for cell 1 and an MEA with pinhole in the middle and end of the cell was used for cell 2.

Table 3. OCV for the PowerCell stack architecture in section 2.2 at different resistance and hydrogen concentration. C# denotes the cell number at which the resistance in the corresponding row was added.

Table 4. OCV for a 3-cell short stack using the Greenlight cell architecture in section 2. A brand new MEA was used for cell 1, a previously conditioned MEA was used for cell 2, and an MEA with pinhole in the middle and end of the cell was used for cell 3. A 10 Ω resistance was placed in parallel with cell 1.

Symbol	*Property*
A	Cell active geometric area, m^2
d	Membrane thickness, m
E	Cell potential, V
F	Faraday constant, 96485 A s mol
T	Cell temperature, K
i_s	Short circuit current, A
K_{H2}	Membrane permeability, $m^2\ s^{-1}$
P_a	Anode pressure, Pa
P_c	Cathode pressure, Pa
$P_{H2,a}$	Anode hydrogen partial pressure, Pa
$P_{H2,c}$	Cathode hydrogen partial pressure, Pa
$P_{w,a}$	Anode vapor partial pressure, Pa
Q_D	Hydrogen diffusion flow rate through membrane, mol s^{-1}
Q_{H2}	Hydrogen crossover flow rate through pinhole, mol s^{-1}
Q_L	Total gas crossover flow rate through pinhole, mol s^{-1}
Q_{N2}	Nitrogen flow rate in cathode, mol s^{-1}
Q_S	Hydrogen production flow rate due to electric short, mol s^{-1}
R	Universal gas constant, 8.31 J mol^{-1} K^{-1}
R_S	Electric short resistance, ohm
S	Leak size, mol s Pa^{-1}
T	Cell temperature, K
x	Hydrogen molar fraction